ELSEVIER

Earth and Planetary Science Letters 179 (2000) 551–565

EPSL

www.elsevier.com/locate/epsl

Seismic anisotropy of South African upper mantle xenoliths

C. Long, N.I. Christensen *

Department of Geology and Geophysics, University of Wisconsin-Madison, Madison, WI 53706, USA

Received 11 February 2000; accepted 21 April 2000

Abstract

Seismic properties of six upper mantle xenoliths from South Africa were determined both by laboratory measurements at elevated pressure and numerical calculations from petrofabric analyses, in order to provide constraints on the structural interpretation of the field seismic data obtained in recent years. The samples studied include harzburgite, garnet harzburgite, mica harzburgite, lherzolite and garnet lherzolite. Average anisotropies calculated from petrofabrics are 5.4% for V_p and 4.4% for V_s. Ultrasonic measured anisotropies from xenolith rock cores are approximately 1% lower than calculated values. This difference is likely due to simplifications in modal mineralogy used in the calculations and small amounts of alteration in the samples used in the velocity measurements. Comparison of laboratory data with the SKS and P_n data yields possible structural orientations in the upper mantle beneath the South Africa continent. Our results suggest that foliation in the upper mantle is likely horizontal, and the stretching lineation (olivine *a*-axis) is oriented N30°E, which coincides with the absolute plate motion (APM) of the South African continent. It is apparent from our data that the fast S-wave polarization depends on the propagation direction with respect to petrofabric orientations and does not always indicate the stretching lineation.

Keywords: anisotropy; upper mantle; velocity; xenoliths; olivine; petrofabrics

1. Introduction

Since Hess [1] first reported evidence of P-wave velocity anisotropy of oceanic upper mantle and proposed that it originated from olivine preferred orientation, both field seismic observations and laboratory studies of upper mantle rock anisotropy have shown that seismic anisotropy is a common feature of the upper mantle. In addition to the observation of azimuthal variations of P_n velocity, several methods have been developed to extract information on upper mantle anisotropy, including P-wave residuals (e.g., [2,3]), SKS splitting (e.g., [4–6]) and Love/Rayleigh-wave incompatibility (e.g., [7,8]). Due to the limitation of the ray path geometry, however, in situ seismic observations cannot provide complete information on the nature of upper mantle anisotropy. For example, the azimuthal variations of P_n velocity yield only P-wave anisotropy in a horizontal plane beneath the Moho, and SKS measurements provide only S-wave splitting parameters in a single direction (usually vertical). However, a combination of seismic observations and laboratory studies of mantle xenoliths provides an important way to

* Corresponding author. Fax: +1-608-262-0693; E-mail: chris@geology.wisc.edu

0012-821X/00/$ – see front matter
PII: S0012-821X(00)00135-7

understand in situ structural orientations of upper mantle minerals.

In recent years, laboratory studies of mantle rock anisotropy have focused on the (1) magnitude and symmetry of velocity anisotropy, (2) relative orientation between seismic properties and the structural framework, and (3) in situ structural orientation with constraints from experimental petrology and seismic observations. In this context, the oceanic upper mantle is much better understood than the continental upper mantle. Detailed investigations on the major ophiolite massifs over the world (e.g., [9,10]) demonstrated that the V_p anisotropy of the oceanic upper mantle varies from 3 to 8%, and the symmetry of olivine fabrics varies from orthorhombic to axial with the axial symmetry axis corresponding to olivine *a*-axes maxima and parallel to spreading direction. It was also found that pyroxene *a*-, *b*-, and *c*-axes maxima are usually parallel to olivine *b*-, *c*- and *a*-axes, respectively, and anisotropy decreases with increasing pyroxene content [10]. It was shown that the symmetry and magnitude of anisotropy depend upon: (1) the volume percentage of the minerals constituting the upper mantle; mainly olivine and pyroxene, (2) the degree and symmetry of preferred orientation of each mineral, and (3) the alignment of the minerals' crystallographic axes relative to one another. Unlike the oceanic upper mantle, surface exposures of continental upper mantle are rare and laboratory studies, therefore, have been essentially based on the mantle xenoliths. Published data show that seismic properties of xenoliths of continental upper mantle origins are surprisingly consistent from place to place, and the magnitude and symmetry of anisotropy are comparable to those obtained from oceanic upper mantle (e.g., [11–13]).

It is evident, however, that the upper mantle is somewhat heterogeneous (e.g., [14]). Therefore, the degree to which the xenolith samples represent the upper mantle is still of major concern. To obtain a reliable average anisotropy or a range of anisotropies for the upper mantle, it is necessary, therefore, to study a large number of samples. Because the xenoliths are often too small and friable to core for direct laboratory measurements, previous values of anisotropy were often obtained from numerical calculations. It is certainly desirable to have laboratory measurements as long as the suitable samples are available, because they provide not only reliable results, but also constraints on the calculated anisotropy data.

South Africa is one of the most productive areas of mantle xenoliths on the Earth's surface, and provides good opportunities for direct assessments of upper mantle rocks. Extensive petrologic studies have been performed on kimberlite nodules from South Africa (e.g., [15]). Mainprice and Silver [11] calculated anisotropies for six kimberlite nodules from petrofabric studies. However, no laboratory measurements have previously been reported for mantle xenoliths from the South African continent. In recent years, many significant seismic investigations have been carried out on the South African continent, including the SKS measurements [16] and the velocity modeling of the upper mantle using regional seismic data [17]. To provide constraints on the interpretation of the SKS and P_n data, we present detailed properties of six xenolith samples collected from Bulfontein, South Africa. Both laboratory measurements and numerical calculations are used in this study, in order to obtain more convincing data. The discrepancies between measured and calculated data and their possible causes are discussed. The laboratory data are compared with the observed SKS delay times and P_n velocities, and possible interpretations are suggested.

2. Xenolith samples

Peridotite xenoliths collected from the Bulfontein Mine, Kimberly, South Africa (Fig. 1) were sampled by Barry Dawson. The inland plateau of South Africa is the region of most concentrated kimberlite intrusions in the world [15], and the intrusions in the Kimberly area have been well described by Hawthorne [18] and Dawson and Hawthorne [19]. Kimberlites at Bulfontein occur in diatremes which intrude Carboniferous–Jurassic sediments. They are lined up along deep-seated fractures which cut across the trend of the basement gneisses [15]. Radiometric ages of the kimberlite pipes are between 80 and 140 Myr. [20,21].

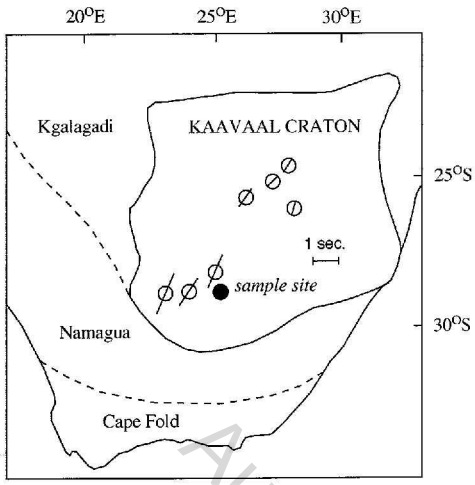

Fig. 1. Location map showing sample site and the results of SKS measurements of Vinnik et al. [16]. The circles are seismic stations used for the SKS measurements. The direction of the fast shear wave polarization at each station is shown by a straight line; the length of the line is proportional to the delay time.

The protracted period of intrusion coincides with a period of strong continental uplift in the Cretaceous [22].

The samples vary from mica peridotite to garnet harzburgite. The modal composition and the general characteristics of these samples are given in Table 1. Samples BD1675, BD3024, BD3659, and BD3661 are unfoliated and display granular textures (Fig. 2). Samples BD1999 and BD3108 exhibit porphyroclastic textures and are foliated. Equant granublastic textures are considered to be common for the peridotite in the upper mantle, especially for the harzburgites [23]. The *P–T* conditions determined from a lherzolite (BD1999) are 980°C and 4.5 GPa, corresponding to approximately 150 km. The temperature of equilibration is estimated using the partition relations for Mg and Fe [24] among olivine, orthopyroxene, clinopyroxene, and garnet, and the pressure is determined from the aluminum content of orthopyroxene in equilibrium with garnet [25]. The peridotite suite from Bulfontein Mine has equilibrated over a very narrow *P–T* interval [15].

Two thin sections were made from each sample for petrofabric measurements using a 5-axis universal stage. Olivine fabrics were measured for all samples, and orthopyroxene fabrics for two samples (BD1675 and BD3108). Measured lattice preferred orientation (LPO) data are presented in Fig. 3 as contoured lower hemisphere, equal-

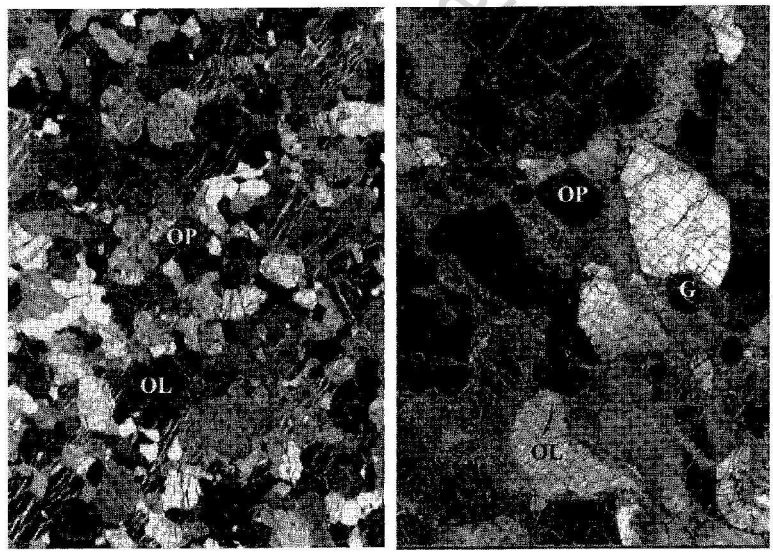

(a) (b)

Fig. 2. Thin section photos showing typical textures of the xenolith samples. The mineral grains marked with 'OP', 'OL' and 'G' are orthopyroxene, olivine and garnet, respectively. The Photo width is 20 mm. (a) Sample BD1675; (b) sample BD 3661.

Table 1
Characteristics of xenolith samples

Sample	Rock type	Modal composition	Texture	Grain size
BD1675	Harzburgite	olivine 60% serpentine 16% orthopyroxene 24%	granular–tabular	~3 mm
BD1999	Garnet–harzburgite	olivine 40% serpentine 28% orthopyroxene 24% garnet 8%	porphyroclastic foliation	2–10 mm (porphyrocrystals) <0.05 mm (matrix)
BD3024	Garnet–lherzolite	olivine 33% serpentine 35% orthopyroxene 15% clinopyroxene 4% garnet 12% mica 1%	granular–tabular some garnet	~5 mm ~10 mm for some garnet crystals
BD3108	Mica–peridotite	olivine 40% serpentine 39% orthopyroxene 10% hornblende 8% mica 3% minor phlogopite and richterite	granular–porphyroclastic foliation	0.5–6.0 mm
BD3659	Harzburgite	olivine 53% serpentine 30% orthopyroxene 17%	tabular–porphyroclastic	~2 mm (matrix) ~10 mm (porphyroclastic)
BD3661	Garnet–harzburgite	olivine 44% serpentine 16% orthopyroxene 32 garnet 7% mica 1%	granular–porphyroclastic	0.1–6.0 mm

area projections. Each diagram consists of measurements of at least 100 grains for olivine and 50–60 grains for orthopyroxene. The olivine fabric pattern for sample BD1675 is characterized by hexagonal symmetry, with strong *a*-axes concentration and *b*- and *c*-axes randomly scattered or weakly oriented in the plane perpendicular to olivine *a*-axes maxima. The olivine fabrics of all other samples are characterized by orthorhombic symmetries.

3. Measured anisotropy

To prepare the samples for velocity measurements, mini-cores of approximately 2.0 cm in diameter and 3.0–3.8 cm in length were made from the rock samples. Due to the limitation of sample size, only two cores were cut for each sample along the maximum preferred orientation of olivine *a*- and *b*-axes, respectively. These two directions are expected to be the fastest (*a*-axis) and slowest (*b*-axis) V_p directions. Compressional and two shear wave velocities polarized at the preferred directions of olivine crystallographic axes were measured on each core at hydrostatic confining pressures up to 1000 MPa, using the pulse transmission technique [26,27] and 1 MHz transducers. The bulk density of each core was calculated from its mass and dimensions.

Measured V_p and V_s at different confining pressures are summarized in Tables 2 and 3, respectively. A typical velocity–pressure curve of this data set is shown in Fig. 4. The results show a considerable range of V_p between the samples. V_p of A-cores (parallel to olivine *a*-axis maxima) at 1000 MPa varies from 6.91 km/s (BD3108) to 7.75 km/s (BD1999), and V_p of B-cores (parallel to

Table 2
Measured compressional wave velocities (V_p, km/s) at different pressures

Sample		Density	Pressures (MPa)									
		(kg/m^3)	20	40	60	80	100	200	400	600	800	1000
BD1675	a	3.168	6.802	7.066	7.228	7.331	7.400	7.539	7.617	7.659	7.689	7.712
	b	3.134	6.222	6.585	6.817	6.971	7.073	7.270	7.348	7.383	7.409	7.428
BD1999	a	3.116	5.880	6.293	6.599	6.832	7.010	7.457	7.652	7.700	7.728	7.750
	b	3.103	5.497	5.901	6.186	6.395	6.552	6.930	7.110	7.177	7.222	7.257
BD3024	a	3.016	4.124	5.000	5.601	6.024	6.325	6.959	7.192	7.274	7.332	7.378
	b	3.014	3.174	4.110	4.775	5.257	5.611	6.410	6.721	6.822	6.891	6.946
BD3108	a	2.976	5.596	5.869	6.067	6.217	6.334	6.638	6.796	6.849	6.883	6.909
	b	2.997	5.902	6.203	6.379	6.486	6.553	6.678	6.748	6.787	6.814	6.836
BD3659	a	3.049	5.268	5.768	6.110	6.351	6.523	6.896	7.046	7.103	7.143	7.174
	b	3.103	5.209	5.720	6.058	6.290	6.450	6.777	6.908	6.963	7.002	7.033
BD3661	a	3.121	6.396	6.862	7.131	7.289	7.385	7.535	7.591	7.620	7.641	7.657
	b	3.126	6.626	6.989	7.174	7.273	7.328	7.415	7.466	7.495	7.516	7.532

olivine *b*-axis maxima) varies from 6.84 km/s (BD3108) to 7.53 (BD3661) km/s. The V_p variation from sample to sample is well correlated with the combination of (1) model composition, especially the serpentine and olivine contents, (2) degree of LPO of olivine and pyroxene, (3) development of foliation/lineation defined by grain shapes and/or compositional zoning. The V_s variation between samples is also apparent and can be understood in the same terms. As expected, V_p along the A-cores is faster than along the B-cores for all samples. For most samples, the fastest V_s is measured along A-cores with a polarization parallel to the olivine *c*-axis maxima, and the slowest V_s is measured along B-cores with a polarization parallel to the olivine *c*-axis maxima.

Due to low temperature mineral alteration of the rock samples (e.g., serpentinization) measured properties do not represent the upper mantle properties unless the proper corrections for the alteration are made. In fact, similar corrections are also necessary in velocity calculations, because some alteration products of South African xenoliths have formed in the upper mantle by metasomatic processes [15]. An example of this is the phlogopite and richterite in sample BD3108 (Table 1).

4. Calculated anisotropy

Seismic properties of rocks can be calculated from single crystal elastic constants, densities, model composition and petrofabrics of constituent minerals. The basics of the method have first been described by Crosson and Lin [28]. This method is particularly useful in studies of ultramafic xenoliths, because they are usually too small and too friable to core for laboratory measurements. In this study, compressional and shear wave velocities, shear wave splitting and fast shear wave polarization directions are calculated from the model composition and the petrofabric data given in previous sections, but serpentine is replaced by olivine and orthopyroxene with respect to the ratio of their contents. The minerals with no fabric data, such as garnet, clinopyroxene, are assumed to be randomly oriented. Shear wave splitting is defined as $\delta V_s = 2(V_{s1} - V_{s2})/(V_{s1} + V_{s2})$, where V_{s1} and V_{s2} are fast and slow shear wave velocities, respectively, for a particular propagation direction. The Hill averaging method has been used for our calculations [29]. Single crystal elastic constants of olivine and their pressure and temperature derivatives are taken from Kumazawa and Anderson [30]. The single crystal data of orthopyroxene and garnet are taken from Frisillo and Barsch [31] and Bonczar et al. [32], respectively. The pressure derivatives for orthopyroxene appear unreasonably high compared to those obtained from laboratory measurements on pyroxenite to 3 GPa [33,34], therefore, a correction was applied accordingly in our calculations. The single crystal data at room temperature and

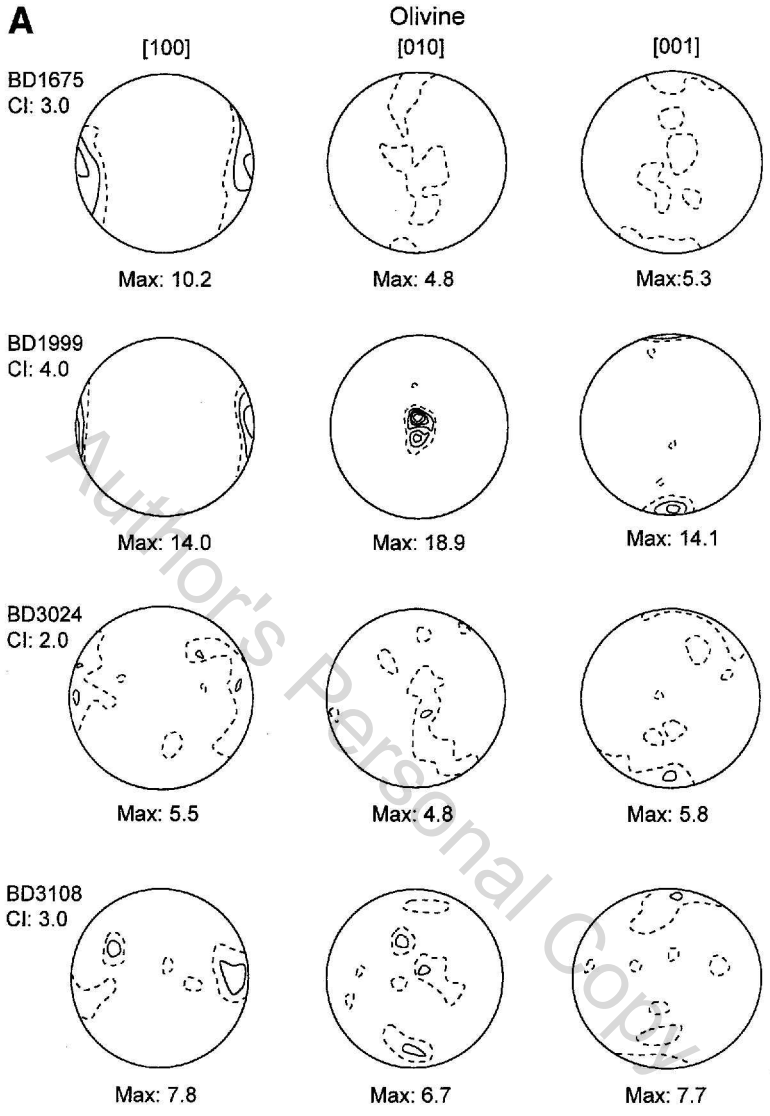

Fig. 3. Equal-area, lower hemisphere projection diagrams showing LPO of olivine and orthopyroxene. Each diagram consists of at least 100 measurements for olivine, and 50–60 for orthopyroxene. Dashed lines are minimum contours. CI denotes contour interval.

pressure of clinopyroxene, hornblende and mica are taken from Levien et al. [35], and Aleksandrov and Ryzhova [36], respectively. Average values at 4 GPa and 950°C, obtained with references to previously published P–T data [11] for the peridotite xenoliths from the same kimberlite pipe, were used for pressure and temperature corrections in the velocity calculations.

The calculated results are presented in Fig. 5, and the contoured diagrams are in the same orientation as the fabric diagrams in Fig. 3. The average values of V_p, V_s, V_p anisotropy and maximum V_s splitting for these samples are 8.33 km/s, 4.75 km/s 5.4% and 4.4%, respectively. The V_p distribution generally shows similar patterns to the olivine fabrics, and for all samples, the maximum and minimum V^p coincide with the preferred orientation of olivine a- and b-axes, respec-

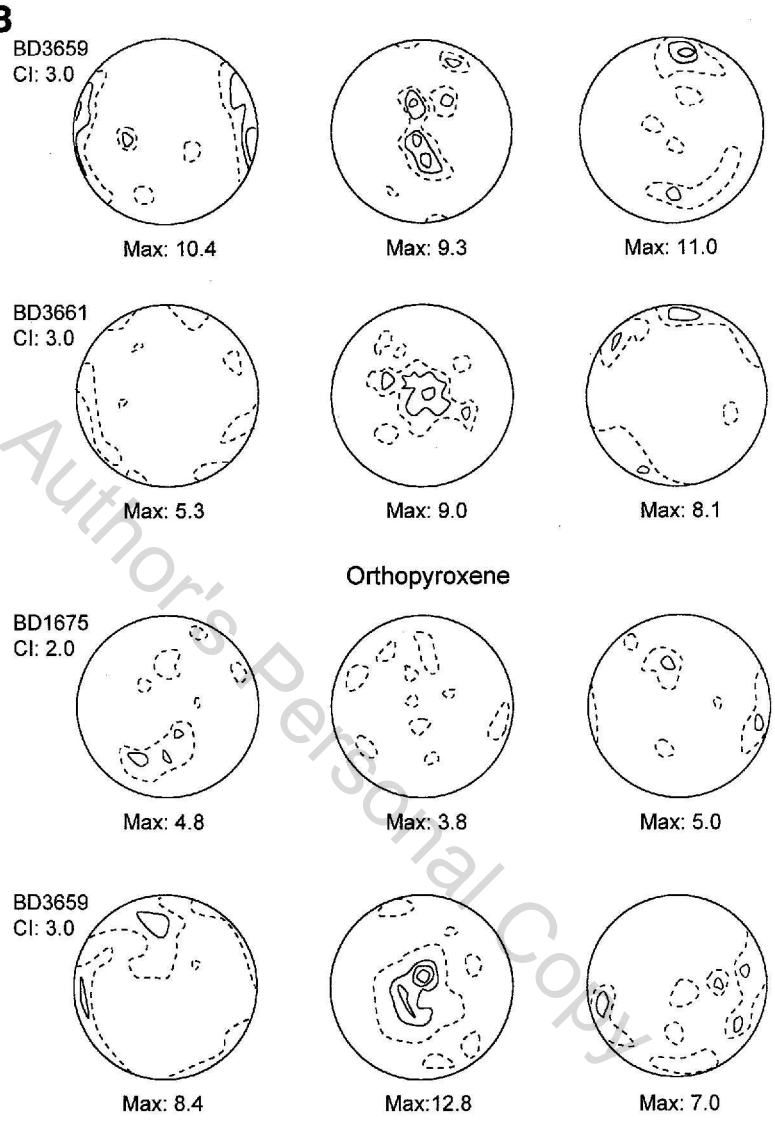

Fig. 3 (*continued*).

tively. The V_S distribution is also directly related to the olivine fabric patterns. The distribution of V_S splitting, however, displays a different and more complicated pattern than that of the olivine fabrics. This seems to be a common phenomena and is physically understandable, simply because the V_S splitting coefficient, unlike velocities, is not a direct product of the elastic constants. The maximum V_S splitting generally occurs at the directions oblique to the olivine crystallographic axes, although it tends to be parallel to olivine *c*-axis maxima. The polarization diagrams in Fig. 5 show clearly that the fast V_S polarization directions vary with propagation directions.

5. Comparison of measured and calculated data

Differences between measured and calculated velocities are often observed for polymineralic ag-

Table 3
Measured shear wave velocities (V_s, km/s) at different pressures

Sample		Density	Pressures (MPa)									
		(kg/m^3)	20	40	60	80	100	200	400	600	800	1000
BD1675	ab[a]	3.168	3.910	4.021	4.083	4.119	4.142	4.189	4.224	4.244	4.258	4.269
	ab		3.694	3.818	3.889	3.932	3.959	4.012	4.047	4.066	4.080	4.091
	ba	3.134	3.802	3.945	4.027	4.076	4.107	4.161	4.188	4.203	4.214	4.222
	bc		3.569	3.707	3.793	3.847	3.882	3.945	3.970	3.982	3.991	3.998
BD1999	ab	3.116	3.405	3.627	3.772	3.871	3.939	4.075	4.131	4.155	4.172	4.186
	ac		3.505	3.700	3.833	3.926	3.991	4.123	4.168	4.183	4.193	4.201
	ba	3.103	3.243	3.423	3.549	3.640	3.706	3.855	3.915	3.935	3.949	3.960
	bc		3.138	3.369	3.527	3.639	3.719	3.894	3.963	3.989	4.007	4.020
BD3024	ab	3.016	3.089	3.265	3.374	3.452	3.511	3.661	3.767	3.823	3.863	3.894
	ac		2.876	3.177	3.355	3.465	3.535	3.669	3.748	3.792	3.823	3.848
	ba	3.014	2.639	2.959	3.182	3.343	3.461	3.730	3.845	3.887	3.916	3.939
	bc		2.575	2.946	3.193	3.362	3.479	3.709	3.787	3.815	3.835	3.851
BD3108	ab	2.976	3.158	3.287	3.373	3.435	3.479	3.583	3.636	3.659	3.676	3.689
	ac		3.195	3.292	3.356	3.400	3.432	3.503	3.538	3.554	3.565	3.574
	ba	2.997	3.492	3.596	3.660	3.702	3.730	3.787	3.818	3.835	3.847	3.856
	bc		3.463	3.520	3.560	3.591	3.614	3.675	3.708	3.719	3.727	3.733
BD3659	ab	3.049	2.801	3.150	3.366	3.503	3.592	3.754	3.822	3.856	3.881	3.900
	ac		3.039	3.295	3.470	3.592	3.678	3.858	3.920	3.941	3.956	3.967
	ba	3.103	2.953	3.237	3.422	3.545	3.627	3.780	3.827	3.845	3.858	3.867
	bc		2.939	3.204	3.388	3.519	3.614	3.826	3.914	3.946	3.968	3.986
BD3661	ab	3.121	3.707	3.823	3.890	3.933	3.963	4.039	4.104	4.142	4.170	4.190
	ac		3.920	4.020	4.078	4.113	4.135	4.181	4.212	4.230	4.243	4.252
	ba	3.126	3.899	3.946	3.975	3.996	4.011	4.054	4.089	4.110	4.124	4.135
	bc		3.849	3.913	3.955	3.988	4.016	4.109	4.201	4.247	4.274	4.292

[a]The first letter denotes propagation direction, and the second vibration direction

gregates. Previous studies show that differences between calculated and laboratory measured velocities and anisotropies vary from sample to sample (e.g., [28,37]). A comparison of our two data sets allows an assessment of the possible causes of these differences. All velocities were reduced to room temperature and pressure. Laboratory velocities at atmospheric pressure were obtained by extrapolations from pressures above 600 MPa (see Fig. 4) where the effects of microfractures and porosity are largely eliminated. The calculated velocities are corrected for serpentine content by:

$$1/V = C_{serp}/V_{serp} + (1-C_{serp})/V_{sf}$$

where C_{serp} is the volume percent of serpentine, V_{serp} is velocity of serpentine, and V_{sf} is the velocity of the serpentine free rock [28,38]. Since single crystal elastic constant data for serpentine have not been measured, velocities of serpentinite

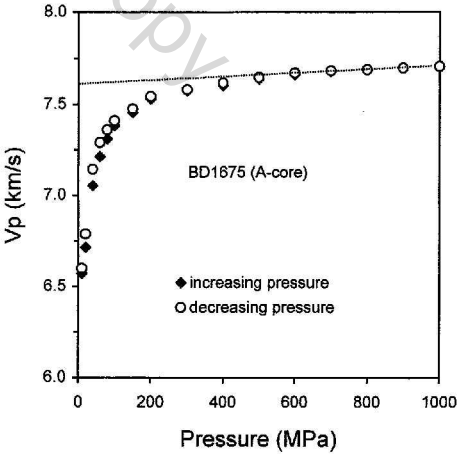

Fig. 4. An example of laboratory measured velocity–pressure curve. Dashed line is linear fit to velocities measured at pressures over 6 kilobars and extrapolation to low pressures.

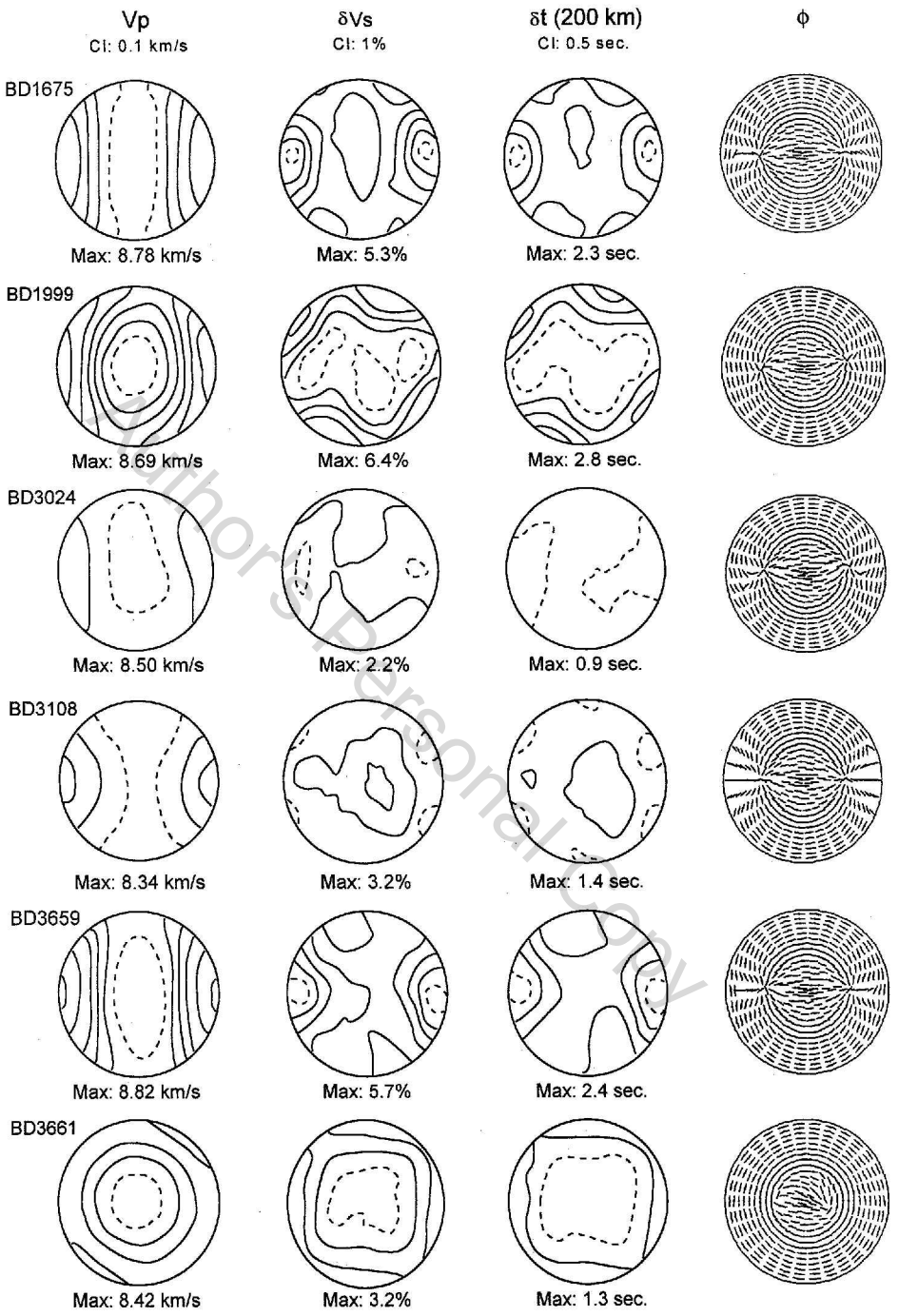

Fig. 5. P-wave velocities (V_p), S-wave splitting coefficients (δV_s, δt), and fast S-wave polarization directions (ϕ) calculated from petrofabric data of olivine and orthopyroxene. The diagrams are in the same orientation as the fabric diagrams in Fig. 3. Dashed lines are minimum contours. CI denotes contour interval.

Table 4
Comparison of measured and calculated velocities

Sample		V_p			V_s		
		calculated	measured	$V_{cal}-V_{mea}$	calculated	measured	$V_{cal}-V_{mea}$
BD1675	-a[a]	7.76	7.57	0.19			
	-b	7.41	7.33	0.08			
	-ab				4.23	4.23	0.00
	-ac				4.24	4.03	0.21
	-bc				4.15	3.96	0.19
BD1999	-a	7.24	7.64	−0.40			
	-b	6.95	7.03	−0.08			
	-ab				3.83	4.00	−0.17
	-ac				3.89	4.16	−0.27
	-bc				3.79	3.92	−0.13
BD3024	-a	7.10	7.08	0.02			
	-b	6.96	6.60	0.36			
	-ab				3.81	3.78	0.03
	-ac				3.82	3.75	0.07
	-bc				3.78	3.77	0.01
BD3108	-a	6.67	6.75	−0.08			
	-b	6.56	6.70	−0.14			
	-ab				3.51	3.70	−0.19
	-ac				3.52	3.53	−0.01
	-bc				3.49	3.70	−0.21
BD3659	-a	7.23	7.00	0.23			
	-b	6.87	6.87	0.00			
	-ab				3.80	3.80	0.00
	-ac				3.82	3.88	−0.06
	-bc				3.72	3.88	−0.16
BD3661	-a	7.66	7.54	0.12			
	-b	7.42	7.42	0.00			
	-ab				4.21	4.07	0.14
	-ac				4.26	4.19	0.07
	-bc				4.19	4.18	0.01

[a]The first letter denotes propagation direction, and the second viberation direction

($V_p = 5.0$ km/s, $V_s = 2.5$ km/s) are used in the correction [39]. Comparisons of the measured and calculated velocities (Table 4) illustrate the following: (1) many of the calculated velocities agree well with the measured velocities, (2) the differences between measured and calculated velocities vary from sample to sample with an average of 1.7% for V_p and 2.1% for V_s, (3) calculated velocities are higher than measured velocities for unfoliated samples (BD1675, BD3024, BD3661, and BD3659) and lower for foliated samples (BD1999 and BD3108).

The accuracy of laboratory velocity measurements using the pulse transmission technique has been rigorously evaluated by Christensen and Shaw [40], and the error is generally regarded to be less than 0.5% for V_p and 1% for V_s. Therefore, the error associated with this technique cannot explain some of the observed velocity differences. Although the accuracies of the fabric measurements and modal analysis are difficult to evaluate, it is expected that with a large number of grains, the measured fabric strength tends to be stabilized. Similarly, modal analysis becomes more reliable by increasing the number of grains and the area counted.

Another possible source of the velocity differences is the presence of structures larger than lattice scales in the rocks, such as foliation and lineation defined by compositional banding and/or

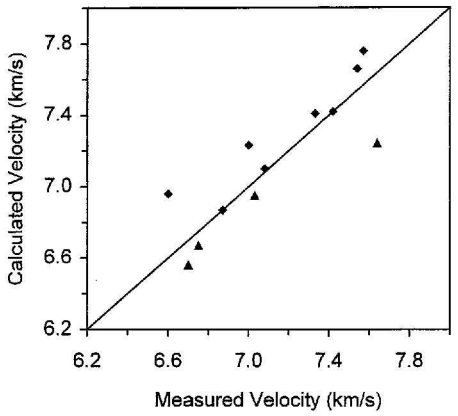

Fig. 6. Comparison of measured and calculated P-wave velocities at room temperature and pressure. Triangles represent foliated samples (BD1999 and BD3108), and diamonds are of unfoliated samples. The straight line is plotted for measured V_p = calculated V_p.

grain shape, because the calculations assume that rocks are uniform in composition and the individual mineral grains are equigranular. A close correlation of the velocity differences with the structures displayed in the rock samples suggests that 'structure-induced error' in the calculations may be significant. Calculated velocities of foliated samples (BD1999 and BD3108) are lower than measured velocities, but calculated velocities of unfoliated samples (BD1675, BD3024, BD3661, and BD3659) are systematically higher than measured velocities (Fig. 6). The good correlation between measured and calculated velocities for a majority of the samples suggests that the Hill average is reasonable for our samples. Other average techniques such as the shear-lag model [41] would improve the agreement for selected samples.

6. Discussion

6.1. Previous studies of xenolith anisotropies

In order to obtain the overall averages of the upper mantle anisotropies, we compiled all the published xenolith data reported over the past

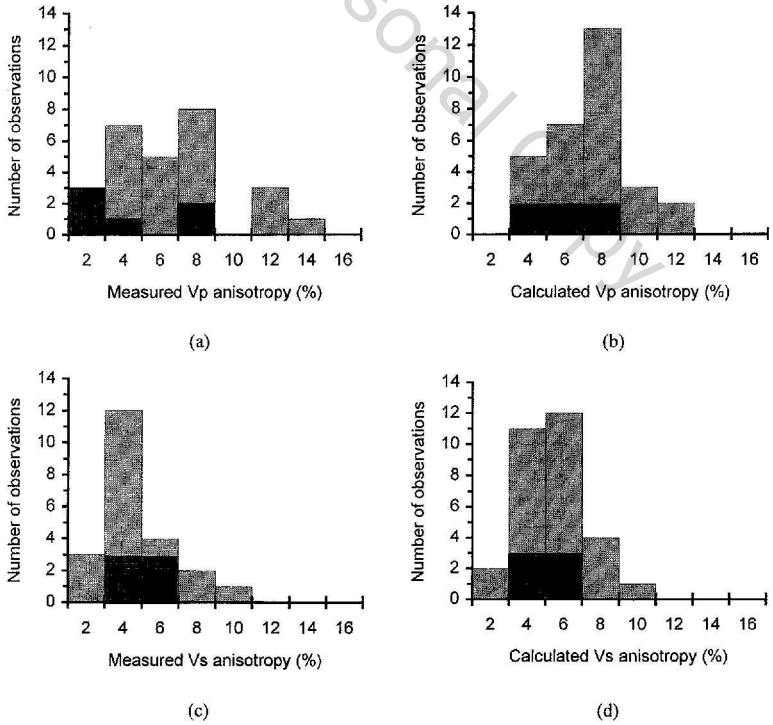

Fig. 7. Histograms showing previous results of xenolith anisotropies. Heavily shaded columns are results from this study.

30 years including data from this study. These results are presented in Fig. 7. This data set includes calculated V_p and V_s anisotropies for 30 xenoliths [11,29,37,42], 27 measured V_p anisotropies [29,37,39,43–45], and 22 measured V_s anisotropies [29,37,39,44]. Compilations of average anisotropies [12,13], where individual sample anisotropies have not been reported, are not included in our figures. The measured anisotropies presented in Fig. 7a,c are at 1.0 GPa and room temperature. The calculated data have been reported for a variety of P–T conditions. However, calculated anisotropies do not vary significantly with pressure and temperature (e.g., [37]).

The measured average anisotropies (5.5% for V_p, 3.5% for V_s) and calculated values (6.3% for V_p, 4.5% for V_s) agree quite well. The calculated anisotropies are slightly higher ($\sim$1%) than measured anisotropies for both V_p and V_s. There are several possible explanations for these differences. Many calculations assume a random orientation for pyroxene in peridotite. Previous studies (e.g., [10]) show that orthopyroxene *a*-, *b*- and *c*-axes maxima parallel the olivine *b*-, *c*- and *a*-maxima, respectively. This relationship produces a lower anisotropy than random pyroxene orientation. On the other hand, laboratory measured anisotropies of peridotite xenoliths are lowered by small amounts of glass (quenched melt [37]), low temperature alteration (e.g., serpentinization with a random crystallographic orientation) and high porosity [44] probably also originating from decompression.

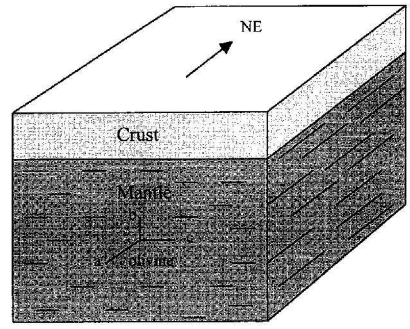

Fig. 8. Olivine preferred orientation in the upper mantle beneath South Africa.

6.2. Comparison of xenolith anisotropy with SKS and P_n anisotropies

Vinnik, et al. [16] measured the SKS delay times and fast V_s polarization directions at seven stations spread over the Kaapvaal Craton (Fig. 1). Their results showed an average delay time (δt) of 1 s and fast S-wave polarization directions (ϕ) at approximately N30°E, which is close to the APM of South Africa plate. They predicted that the V_s anisotropy of the upper mantle is 2%, given an anisotropic layer thickness of 250 km. To provide constraints on the interpretation of observed SKS data, we have calculated possible layer thicknesses for various propagation directions based on our mantle xenolith anisotropies and the observed SKS delay time (Table 5). Our results show that the predicted layer thicknesses vary greatly with propagation direction. Although the thinnest

Table 5
V_s splitting along anisotropic symmetry axes and calculated anisotropic layer thickness with $\delta t = 1$ s

Sample	*a*-axis				*b*-axis				*c*-axis				Maximum splitting	
	V_s1	V_s2	δV_s (%)	h (km)	V_s1	V_s2	δV_s (%)	h (km)	V_s1	V_s2	δV_s (%)	h (km)	δV_s (%)	h (km)
BD1675	4.77	4.76	0.2	2271	4.76	4.65	2.3	201	4.77	4.65	2.5	185	5.1	93
BD3569	4.85	4.79	1.2	387	4.79	4.59	4.3	110	4.85	4.59	5.5	86	5.9	81
BD3108	4.70	4.62	1.7	271	4.62	4.57	1.1	422	4.70	4.57	2.8	165	3.2	148
BD3024	4.81	4.80	0.2	2309	4.80	4.70	2.1	226	4.81	4.70	2.3	206	2.5	190
BD3661	4.83	4.72	2.3	207	4.72	4.67	1.1	441	4.83	4.67	3.4	141	3.4	140
BD1999	4.87	4.74	2.7	178	4.74	4.62	2.6	182	4.87	4.62	5.3	90	6.3	75
Average	4.81	4.74	1.5	326	4.74	4.63	2.3	200	4.81	4.63	3.8	124	4.4	108

V_s1 = fast V_s, V_s2 = slow V_s, $\delta V_s = V_s$ splitting, h = anisotropic layer thickness.

layer predicted for the maximum splitting direction may be considered as a lower bound, a more specific range of slab thickness cannot be determined without additional constraints. From studies of experimental petrology (see [12] for a review) and observation seismology (e.g., [46]), it is generally accepted that an anisotropic layer of about 200 km thick within the upper mantle is reasonable and observed SKS delay time mainly originates in this layer. If this is the case, our results indicate that the SKS ray path is possibly parallel or subparallel to olivine *b*-axes maxima, and the fast S-wave polarization parallel to olivine *a*-axes maxima (Fig. 8). This model gives rise to a subhorizontal foliation, which is consistent with the 3-D tomographic model of shear-wave velocity anisotropy in Precambrian cratons of Ekstrom and Dziewonski [47].

The recent study of upper mantle velocity structure of South Africa by Zhao et al. [17] obtains a P-wave velocity of 8.38 km/s at 150 km depth. This velocity is an average value for approximately horizontal propagations, and it is in excellent agreement with the average laboratory V_p (8.40 km/s) in the foliation plane (a–c plane) of our samples supporting a horizontal foliation model for the region.

7. Conclusions

Seismic properties of six kimberlite nodules collected from the Bulfontein Mine, South Africa, were determined by laboratory measurements and numerical calculations from the LPO data of olivine and orthopyroxene. By interpolating to in situ *P–T* conditions (4 GPa, 950°C; approximately 150 km in depth), we obtain average properties of V_p (8.31 km/s), V_s (4.75 km/s), V_p anisotropy (5.4%), and maximum V_s splitting (4.4%). Our data show that effective elastic symmetries of individual samples are mainly controlled by their olivine fabric patterns and that axial symmetry is common with a symmetry axis parallel to olivine *a*-axis maximum concentrations. While the velocities are directly related to the effective elastic constants, the V_s splitting usually shows a different more complicated pattern. The maximum V_s splitting generally occurs at directions close to olivine *c*-axes maxima.

Differences between calculated velocities and measured velocities may originate from several sources. Structures larger than lattice scales in the rocks, such as foliation and lineation defined by compositional banding and/or grain shape influence anisotropies [48,49]. Velocity calculations assume uniform distributions of mineral grains and equigranular textures. Therefore, the higher anisotropies are expected from laboratory measurements on relatively large volume rock cores, which sample layering and grain shape as well as LPO. On the other hand, the calculated velocities and anisotropies may be higher than the measured velocities and anisotropies due to simplifications in modal mineralogy used in the calculations and small amounts of alteration and porosity in the samples used in the velocity measurements.

Measured SKS delay times show much variation on the global scale, usually ranging between 0 and 2 s. This variability likely results from various sources including variations in anisotropic layer thicknesses, magnitude of rock anisotropy, and in situ orientations of anisotropy symmetry. Because the anisotropy of most xenoliths falls in a narrow range (Fig. 7), delay time variations likely reveal lateral variations of structural orientation in the upper mantle. The fast V_s polarization is not necessarily in the direction of stretching lineation (Figs. 3 and 5). Based on the SKS and P_n data measured in the Kaavaal Craton and the properties of upper mantle xenoliths obtained in this study, a likely in situ structural orientation of upper mantle foliation is horizontal/subhorizontal, i.e. the preferred orientation of olivine *b*-axes is vertical or subvertical, and the fast V_s polarization parallels the stretching lineation (olivine *a*-axes maxima).

Acknowledgements

We thank Barry Dawson for providing the xenolith samples. Helmut Durrast and D. Stanley provided constructive comments on an earlier draft of this paper.*[AC]*

References

[1] H.H. Hess, Seismic anisotropy of the upper mantle under oceans, Nature 230 (1964) 629–631.

[2] A.M. Dziewonski, D.L. Anderson, Travel times and station corrections for P-waves at teleseismic distances, J. Geophys. Res. 88 (1983) 3295–3314.

[3] V. Babuska, J. Plomerova, J. Sileni, Large-scale orientated structures in the subcrustal lithosphere of Central Europe, Ann. Geophys. 2 (1984) 649–662.

[4] L.P. Vinnik, G.L. Kosarev, L.I. Makeyeva, Anisotropy in the lithosphere from the observations of SKS and SKKS, Proc. Acad. USSR 78 (1984) 1335–1339.

[5] L.P. Vinnik, Veronique Farra and Barbara Romanovicz, Azimuthal anisotropy in the earth from observation of SKS at GEOSCOPE and NARS broadband stations, Bull. Seism. Soc. Am. 79 (1989) 1542–1558.

[6] P.G. Silver, W.W. Chan, Implications for continental structure and evolution from seismic anisotropy, Nature 335 (1988) 34–39.

[7] D.W. Forsyth, The early structure evolution and anisotropy of the oceanic upper mantle, Geophys. J. R. Astron. Soc. 33 (1975) 103–162.

[8] J.P. Montagner, T. Tanimoto, Global upper mantle tomography of seismic velocities and anisotropy, J. Geophys. Res. 96 (1991) 20337–20351.

[9] N.I. Christensen, M.H. Salisbury, Seismic anisotropy in the oceanic upper mantle: evidence from the Bay of Islands ophiolite complex, J. Geophys. Res. 84 (1979) 4601–4610.

[10] N.I. Christensen, The magnitude, symmetry and origin of upper mantle anisotropy based on fabric analyses of ultramafic tectonites, Geophys. J. R. Astron. Soc. 76 (1984) 89–111.

[11] D. Mainprice, P.G. Silver, Interpretation of SKS-waves using samples from the sub continental lithosphere, Phys. Earth Planet. Int. 78 (1993) 257–280.

[12] S. Ji, X. Zhao, D. Francis, Calibration of shear-wave splitting in the subcontinental upper mantle beneath active orogenic belts using ultramafic xenoliths from the Canadian Cordillera and Alaska, Tectonophysics 239 (1994) 1–27.

[13] W.B. Ismail, D. Mainprice, An olivine fabric database: an overview of upper mantle fabric and seismic anisotropy, Tectonophysics 296 (1998) 145–157.

[14] S. McGeary, M.R. Warner, Seismic profiling the continental lithosphere, Nature 317 (1985) 795–797.

[15] J.B. Dawson, Kimberlites and their xenoliths, Springer-Verlag, New York, 1980, 258 pp.

[16] L.P. Vinnk, R.W.E. Green, L.O. Nicolaysen, Recent deformations of the deep continental root beneath southern Africa, Nature 375 (1995) 50–52.

[17] M. Zhao, C.A. Langston, A.A. Nyblade, Upper mantle velocity structure beneath southern Africa from modeling regional seismic data, J. Geophys. Res. 104 (1999) 4783–4794.

[18] J.B. Hawthorne, Kimberlite sills, Trans. Geol. Soc. S. Afr. 71 (1968) 291–311.

[19] J.B. Dawson, J.B. Hawthorne, Magmatic sedimentation and carbonititic differentiation in kimberlite sills at Benfontein, South Africa, J. Geol. Soc. Lond. 129 (1973) 61–85.

[20] G.L. Davis, The ages and uranium contents of zircons from kimberlites and associated rocks, Ext. Abst., 2nd Int. Conf. Kimberlite, Santa Fe, 1977.

[21] A.J. Erlank, N. Schimizu, Strontium and strontium isotope distributions in some kimberlite nodules and minerals, Ext. Abst., 2nd Int. Conf. Kimb., Santa Fe, 1977.

[22] E. Dingle, Mesozoic palaeogeography of the southern Cape, South Africa, Palaeogeogr. Paleaoclimatol. Palaeoecol. 13 (1973) 203–213.

[23] J.C.C. Mercier, A. Nicolas, Textures and fabrics of upper-mantle peridotites as illustrated by xenoliths from basalts, J. Petrol. 16 (1975) 454–487.

[24] A.A. Finnerty, F.R. Boyd, Evaluation of thermobarometers for garnet peridotite, Geochim. Cosmochim. Acta 48 (1984) 15–27.

[25] I.D. MacGregor, The System MgO–Al_2O_3–SiO_2: solubility of Al_2O_3 in enstatite for spinel and garnet peridotite compositions, Am. Mineral. 59 (1974) 110–119.

[26] F. Birch, The velocity of compressional waves in rocks to 10 kilobars, 1, J. Geophys. Res. 65 (1960) 1083–1102.

[27] N.I. Christensen, Compressional wave velocities in metamorphic rocks at pressures to 10 kilobars, J. Geophys. Res. 70 (1965) 6147–6164.

[28] R.S. Crosson, J.W. Lin, Voigt and Reuss prediction of anisotropic elasticity of Dunite, J. Geophys. Res. 76 (1971) 570–578.

[29] B. Soedjatmiko, N.I. Christensen, Seismic anisotropy under extended crust: evidence from upper mantle xenolith, Cima Volcanic Field, California, Tectonophycics, in press.

[30] D.E. Kumazawa, O.L. Anderson, Elastic moduli, pressure derivatives, and temperature derivatives of single-crystal olivine and single-crystal fosterite, J. Geophys. Res. 74 (1969) 5961–5972.

[31] A.L. Frisillo, G.R. Barsch, Measurement of single crystal elastic constants of bronzite as a function of pressure and temperature, J. Geophys. Res. 77 (1972) 6360–6384.

[32] L.J. Bonczar, E.K. Graham, H. Wang, The pressure and temperature dependence of the elastic constants of pyrope garnet, J. Geophys. Res. 82 (1977) 2529–2534.

[33] C. Wang, Pressure coefficient of sound velocity for several rocks (Abstract), EOS Trans. AGU 54 (1973) 473.

[34] N.I. Christensen, Compressional wave velocities in possible mantle rocks to pressures of 30 kilobars, J. Geophys. Res. 79 (1974) 407–412.

[35] L. Levien, D.J. Weidner, C.T. Prewitt, Elasticity of dioside, Phys. Chem. Miner. 4 (1979) 105–113.

[36] K.S. Aleksandrov, T.V. Ryzhova, The elastic properties of rock forming minerals II: Layered silicates, Phys. Solid Earth (1961) 1165–1168.

[37] H. Kern, L. Burlini, I.V. Ashchepkov, Fabric-related seis-

mic anisotropy in upper-mantle xenoliths: Evidence from measurements and calculations, Phys. Earth Planet. Int. 95 (1996) 195–209.
[38] Francis Birch, Elasticity of igneous rocks at high temperatures and pressures, Bull. Geol. Soc. Am. 54 (1943) 263–286.
[39] N.I. Christensen, Elasticity of ultrabasic rocks, J. Geophys. Res. 71 (1966) 5921–5931.
[40] N.I. Christensen, G. Shaw, Elasticity of mafic rocks from the mid-Atlantic ridge, Geophys J. R. Astron. Soc. 20 (1970) 271–284.
[41] Shaocheng Ji, Zichao Zhang, Elastic properties of forsterite-enstatite composites up to 3.0 GPa, J. Geodyn. 28 (1999) 147–174.
[42] L. Peselnick, J.P. Lockwood, R. Stewart, Anisotropic elastic velocities of some upper mantle xenoliths underlying the Sierra Nevada batholith, J. Geophys. Res. 82 (1977) 2005–2010.
[43] D.E. Kumazawa, T. Masaki, Elastic properties of eclogite xenoliths, J. Geophys. Res. 76 (1971) 1231–1243.
[44] V. Babuska, Elastic properties of ultrabasic xenoliths at pressures of up to 10 kb, Phys. Solid Earth 13 (1976) 366–372.
[45] S.Y. O'Reilly, I. Jackson, C. Bezant, Equilibrium temperature and elastic wave velocities for upper mantle rocks from eastern Australia: Implications for interpretation of seismological models, Tectonophysics 185 (1990) 67–82.
[46] P.G. Silver, W.W. Chan, Shear wave splitting and subcontinental mantle deformation, J. Geophys. Res. 96 (1991) 16429–16454.
[47] G. Ekstrom, A.M. Dziewonski, The unique anisotropy of the Pacific upper mantle, Nature 394 (1998) 168–172.
[48] G.W. Postam, Wave propagation in a stratified medium, Geophysics 20 (1955) 780–806.
[49] P.J. Melia, R.L. Carlson, An experimental test of P-wave anisotropy in stratified media, Geophysics 49 (1984) 374–378.